LASER RANGING FOR EFFECTIVE AND ACCURATE TRACKING OF SPACE DEBRIS IN LOW EARTH ORBITS

Guillaume Blanchet[(1)], Hervé Haag[(1)], Laurent Hennegrave[(1)],
François Assémat[(1)], Sophie Vial[(1)], Etienne Samain[(2)]

[(1)] *Astrium SAS, 51-61, Route de Verneuil BP 3002, 78133 Les Mureaux Cedex France,*
Email: firstname.name@astrium.eads.net
[(2)] *Géoazur, Observatoire de la Cote d'Azur, 2130, Route de l'Observatoire, Caussols,*
06460 Saint Vallier de Thiey France, Email: etienne.samain@obs-azur.fr

ABSTRACT

The paper presents the results of preliminary design options for an operational laser ranging system adapted to the measurement of the distance of space debris. Thorough analysis of the operational parameters is provided with identification of performance drivers and assessment of enabling design options.

Results from performance simulation demonstrate how the range measurement enables improvement of the orbit determination when combined with astrometry.

Besides, experimental results on rocket-stage class debris in LEO were obtained by Astrium beginning of 2012, in collaboration with the Observatoire de la Côte d'Azur (OCA), by operating an experimental laser ranging system supported by the MéO (Métrologie Optique) telescope.

1 CHALLENGES OF THE DEBRIS ISSUE

The past decade has been the time for a growing interest for the debris issue, especially in Europe. The subsequent awareness of the inherent risk it carries has, and is still raising major concerns about sustainability of space. Common applications, like satellite imagery, weather forecast or simply global communication are directly threatened by the increasing population of objects on the Earth orbits. The Low Earth Orbit (LEO) is at particular stake with the highest density and variety of objects. The most pessimistic scenarios even predict that the next sever on-orbit events, e.g. satellite collision, might turn into a chain-reaction leading to a massive generation of debris with a dramatic impact on ability to carry on exploitation of space [1].

The prospective system and technology studies conducted by the agencies worldwide are seeking for the right solution in front of that global challenge. Solving the equation is definitely leading to the need for a huge Space Surveillance and Tracking system (SST), combining technologies and delivering sufficient measurement capability to cope with the driving parameters: coverage, timeliness and accuracy. Radar and passive optical technologies are the main contributors in the intended SST architectures. Focusing on the population in LEO, the radar systems provide effective capability as they deliver good accuracy with limited observation and do almost not suffer from weather conditions. Weakness of the radar systems is in their cost and technical complexity. Besides, the passive optical systems offer a cheaper alternative and can preferably support the tracking operations in the upper orbits of the LEO. However, these systems limit measurement to 2-angles data, typically Right-ascension and Declination (Ra/Dec), and suffer from a high dependency on favourable weather, seeing and lighting conditions. Then, resulting effectiveness and accuracy are directly constrained by the opportunity for long paths observation and high revisit rate.

Improvement of the space situation awareness and confidence in assessment of the risk for conjunction requires accurate and timely orbit data. In that prospect, alternative technologies able to deliver responsive and accurate measurements of object position, for limited complexity and cost, would bring new perspectives. The Satellite Laser Raging (SLR) is part of these promising technologies.

2 LASER RANGING PRINCIPLES

Main benefit in the use of laser ranging is ability to measure the radial distance between the observation site and the target object. This radial distance enables significant improvement of the orbit determination

2.1 From time to distance

Laser ranging technology is based on emission of a pulse laser beam from a ground telescope toward an orbiting target and detection of the returned laser photons back to the source after reflection on the target. The range of the target is deduced from measurement of the flight time, back and forth, of the laser pulse considering the relevant propagation model.

Final accuracy of the range measurement depends on estimation and correction of the various effects, which apply on the laser wave as it goes through the system,

at both emission and detection, and the atmosphere. Fig. 1 depicts the key parameters involved in the implementation of satellite laser ranging.
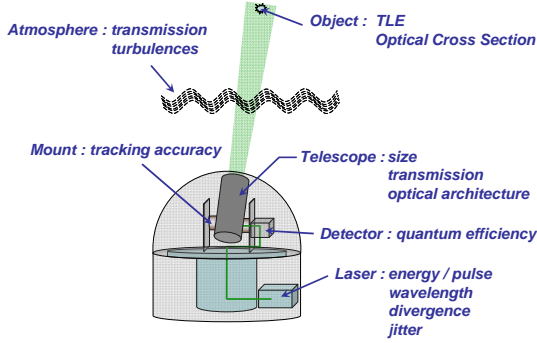
Figure 1. SLR parameters

2.1 link budget issues

The number of detected photoelectrons per transmitted laser pulse is estimated by Eq. 1, known as the classical radar-link equation [2]:

$$N_{pe} = \eta_q . E_0 . \frac{\lambda}{h.c} . \eta_T . G_T . \sigma_{Sat} . \left(\frac{1}{4\pi R^2}\right)^2 . A_R . \eta_R . T_A^2 \quad (1)$$

where:

η_q is the detector quantum efficiency
E_0 is the energy per laser pulse (J)
G_T is the laser/telescope coupling coefficient
σ_{Sat} is the object Optical Cross Section (OCS) (m²)
R is the slant range to the target, obtained by TLE (m)
A_R is the effective area of the receiving telescope (m²)
η_T is the efficiency of the transmitting telescope
η_R is the efficiency of the receiving telescope
T_A is the one way atmospheric transmission, analytically modelled by the Rozenberg equation which takes into account the mass of air X crossed by the laser beam as a function of the zenith angle θ_Z:

$$T_{Atm} = (1 - A_{Atm})^X \quad (2)$$

with

$$X = \frac{1}{\cos\theta_Z + 0.025 . \exp(-11.\cos\theta_Z)} \quad (3)$$

The parameter A_{Atm} is adjusted in order to fit with FASCODE modelling, performed for different atmospheric configurations.

Note that the transmitter gain at the observation point (r_1, θ_1) is defined as [3]:

$$G_T(r_1, \theta_1) = \frac{I(r_1, \theta_1)}{I_0} \quad (4)$$

where $I_0 = 1/4\pi r_1$ is the total intensity for a unit power isotropic source [W/m²] and $I(r_1, \theta_1)$ is the intensity distribution at the observation point [W/m²], modelled by taking into account the divergence of the laser beam and the pointing error of the telescope. The laser/telescope coupling coefficient G_T is obtained by considering the pointing error of the telescope and the divergence of the laser beam (typically a few arc-seconds in both cases).

To estimate the probability of detection, we assume that creation of the primary electrons in a Single Photon Avalanche Diode detector (SPAD) is Poisson distributed [4].

For a laser radar system using Geiger mode Avalanche PhotoDiode (APD), creation of the primary electrons comes from both signal and noise photoelectrons. Since background and dark current statistics also follows a Poisson law, the distributions of created photoelectrons between times t1 and t2 are additive. Therefore, the probability of detection per pulse can be expressed by Eq. 5:

$$P_d = 1 - e^{-(N_S + N_N)} \quad (5)$$

where N_S and N_N represent the mean signal and noise primary photoelectrons generated during the measurement interval, respectively. Note that the mean noise count $N_N = N_B + N_D$ consists of both background and dark current photoelectrons.

3 TARGET TYPOLOGY

A major parameter of the link budget is the Optical Cross Section (OCS), which represents the portion of light reflected from an illuminated object. The OCS of the non-cooperative objects can be computed from their BRDF (Bidirectional Reflectance Distribution Function), which allow characterizing the complex surface of an object and associated diffuse reflection.

In this study, the BRDF is estimated by using the Steinvall model. Aluminium and graphite properties are considered as these materials are the most commonly used in the satellite industry and because their BRDF corresponds to relevant envelopes. Then assumption of spherical object is made for computation of Fig. 3.

Thus, the minimum OCS value for a 10 cm object can be fixed to 0,1 m². With similar approach, typical OCS of a rocket body is estimated between 20 and 50 m². It is therefore possible to deduce the energy per pulse that is required to detect an object of the class of a rocket body in LEO.
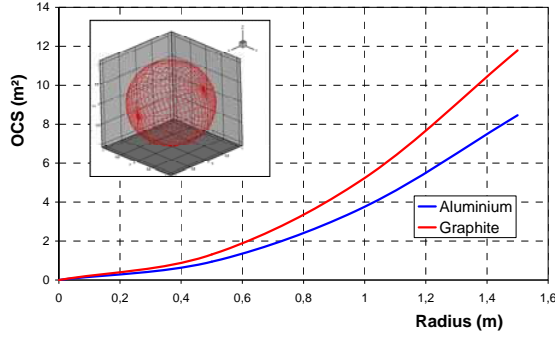
Figure 3. OCS value as a function of radius for spherical objects

4   INFLUENCE OF PARAMETERS

In the prospect to determine drivers for the sizing of a laser ranging station, we evaluate influence of the beam broadening, beam wandering, laser divergence, atmospheric turbulences and telescope aperture and central occultation. Influence of the other parameters is not studied as they mainly generate a linear dependence on the probability of detection per second, which is the probability of detection per pulse multiplied by the repetition rate of the laser source.

The link budget is estimated for the following values:
Total tracking accuracy: 4 Arcsec = 20 µrad
Power of the laser source = energy per pulse x repetition rate = 150 W with 5-10 nanosecond pulses
$\Phi_{\text{Receiving telescope}}$ = 0.7 m
η_{DTC} = 0.4
T_{Emission} = 0.6
$T_{\text{Reception}}$ = 0.3
Object: OCS = 0.1 m², alt = 1000 km, elevation = 25°

4.1   Wavelength

Historically, APD for the short wavelengths, i.e. the more energetic, were favoured as providing higher sensitivity. Thus, most of the SLR stations are working with doubled frequency Nd:YAG lasers. But recently, long wavelengths APD were developed for LIDAR applications, using Nd:YAG lasers, so that performance delivered at 1.06 µm is now comparable to what can be obtained at 532 nm.

Several advantages exist with using the Nd:YAG laser on its fundamental wavelength: a better atmospheric transmission and a lower sensibility to turbulences is provided and losses due to the frequency doubling process are avoided. In addition, diffraction effects induce a two times larger laser spot at 1.06 µm, which reduces the requirement on the tracking accuracy.

Following those considerations, the 1.06 µm wavelength is advocated.

4.2   Beam broadening, wandering and divergence

These three parameters are linked by the design trade-off necessary to achieve realistic and affordable sizing of the SLR system. First idea is to optimize the uplink energy by limiting the laser spot on the target. On the other hand, the requirement on the wandering limit increases. Consistency between the broadening, including divergence, and the wandering parameters is at stake to ensure proper link budget. These parameters shall be kept within a few arc-seconds in all cases.

Therefore, an optimum in the laser beam divergence can be computed, provided assumptions on the two other parameters, and looking for the maximum number of detected photo-electrons. Fig. 4 gives the maximum number of detected photo-electrons as a function of the laser beam divergence.
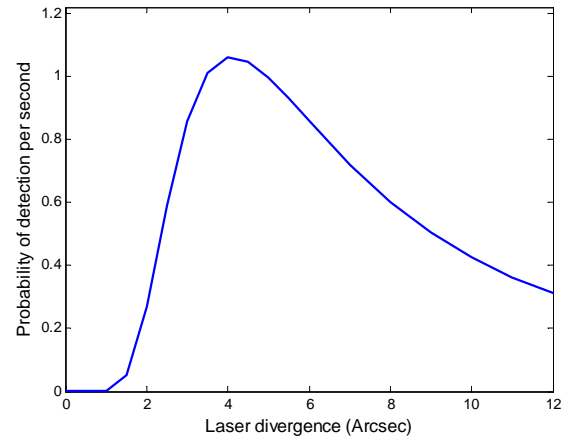
Figure 4. Influence of the divergence of the laser beam on the link budget

For laser low divergence, the target is less illuminated because of the wandering of the laser spot. For laser high divergence, the number of detected photo-electrons decreases because of the spreading of the laser spot.

4.3   Atmospheric turbulences

The influence of the atmospheric turbulences on the beam broadening and the beam wandering has been modelled by taking into account the refractive-index structure constant C_n^2. Its variation as a function of the altitude can be estimated by the so-called SLC-N model [5] and a coefficient α relating to the experimental atmospheric conditions, as defined by Eq. 8:

$$C_n^2(h) = \alpha . C_n^2 \_ SLCN(h) \qquad (8)$$

Considering excellent system performance, to limit the induced impacts on the broadening and wandering

parameters, the effect of the atmospheric turbulences on the link budget can be estimated as shown on Fig. 5.
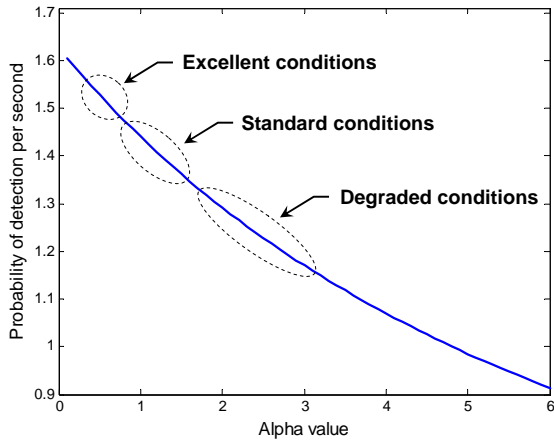
Figure 5. Influence of atmospheric turbulence on link equation

Degraded atmospheric conditions (wind > 50 km/h) may decrease the link budget by up to 25 %.

4.4 Telescope aperture (emission)

It is possible to estimate the influence of the emitting telescope aperture on the mean number of detected photo-electrons. Here, the Fried's analysis fits well with assumption that the atmospheric turbulences limit the influence of the diffraction for telescopes diameters higher than the Fried's parameter r_0.

Fig. 6 shows the mean number of detected photo-electrons as a function of the aperture of the emitting telescope, considering similar broadening and wandering parameters.
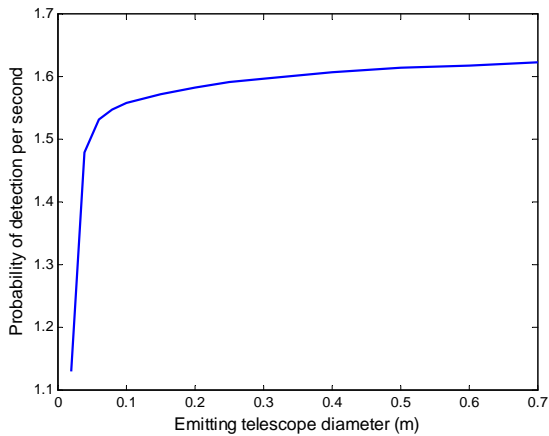
Figure 6. Influence of the diameter of the emitting telescope on the link budget

Thus, for link budget purpose, there is no use to have an emitting telescope with aperture larger than 0.3 m.

4.5 Telescope central occultation

The central occultation of the telescope significantly affects the link budget by addition of the decrease of the collecting area and the laser/telescope coupling.

Fig. 7 shows the mean number of detected photo-electrons as a function of the central occultation for an aperture of 0.25 m.
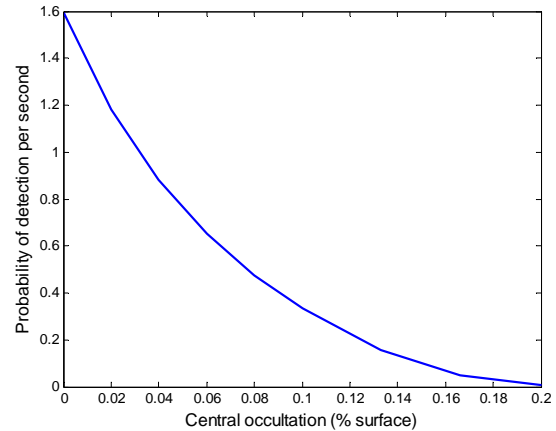
Figure 7. Effect of the central occultation of the telescope on the link budg et (emitting and receiving telescopes identical)

If the emitting and receiving telescopes are identical, it is observed than a 10% central occultation lowers the link budget by more than 75%. If the emitting and receiving telescopes are different, a 10% central occultation lowers the link budget by almost 40%. Thus, central occultation shall be considered as a key design driver for the emitting part of the system.

6   DESIGN DRIVERS FOR EFFECTIVE SLR

The design of an effective SLR station shall optimise its capability of detection, but shall also take into account the material and the maintenance costs induced by a regular employment.

6.1 Performance criteria

According to the conclusions of the §4, a good compromise is obtained with the following set of parameters:
Laser divergence = Total tracking error = 4 Arcsec
$\lambda = 1.06$ µm
$\Phi_{Emitting\ telescope} = 0.25$ m
$\Phi_{Receiving\ telescope} = 0.7$ m
Central obstruction < 7 % (surface)

The highlighting is given to the tracking error, rather than on the laser energy or on the diameter of the receiving telescope. With the above values, a 150 – 200W pulsed laser is required to detect more than one

photon per second (for a 10 cm object at 1000 km with a maximum elevation of 25°).

6.2 Architecture trade-off

Laser ranging systems can be mono-axial (same telescope for the emission and the reception) or bi-axial (two different telescopes). The trade-off analysis considers the following architectures:
- mono-axial system with full pupil
- mono-axial system with pupil sharing
- bi-axial system.

The mono-axial/full pupil and the mono-axial/pupil sharing architectures have roughly the same link budget. Indeed, the losses induced by the central obstruction of the telescope corresponds to the losses dues to the sharing of the aperture. The advantage of the pupil sharing is that the detection module is located on a fixed bench, and that the alignment error of the coudé mirrors is optically corrected. Therefore, the pupil-sharing architecture has potentially a better performance than the full-pupil solution.

Intrinsically, the bi-axial concept has better performances than the pupil-sharing architecture because the emitting and the receiving telescopes can be specifically designed. The misalignment probability of the bi-axial solution is slightly bigger than for the pupil-sharing solution, but is still at a reasonable level because both telescopes are mechanically interdependent.

Depending on the architecture of the emitting telescope, the performances of the bi-axial architecture are about 15 to 20% higher than those of the pupil-sharing solution. Nevertheless, the bi-axial solution is also more expensive, due to additional material and maintenance costs.

Therefore, the mono-axis solution with a shared pupil should optimise the total cost to performance ratio.

7 ENHANCED ORBIT DETERMINATION

The benefit of the SLR measurements can be assessed by simulation. Starting from standard Ra/Dec measurements with associated accuracy, result of the orbit determination (OD) is analysed with and without consideration of the additional range measurements. The measurement noise and rate largely influence the final position and velocity accuracy, as well as the OD convergence speed.

7.1 Simulation parameters

The orbit determination computation is based on tracking data, assuming a preliminary orbit of the target is provided and corresponds to the standard NORAD Two-Line Elements (TLE). The initial uncertainties on the object position and velocity are defined according to estimation of the TLE uncertainties presented in [6]. The diagonal terms – Radial (R), In-track (I) and Cross-track (C) – of the initial uncertainty matrix are defined as in Tab. 1, the others terms are set null.

R_sigma	10 000 m
I_sigma	10 000 m
C_sigma	300 m
Rdot_sigma	140 m/s
Idot_sigma	7 m/s
Cdot_sigma	0.5m/s

Table 1. Diagonal terms of the initial uncertainty matrix

The angular measurements (Ra/Dec) are provided with a fixed frequency set to 0.5 Hz. The angular parameters are equal on both coordinates and set as in Tab. 2.

Bias	0.3 arcsec
Bias_sigma	0.03 arcsec
White_noize_sigma	2.5 arcsec

Table 2. Optical measurement parameters

The range measurements are provided with different accuracies and frequencies as paired in Tab. 3.

Nominal SLR	6 m	0.5 Hz
High-accuracy SLR	0.3 m	0.5 Hz
High-Frequency SLR	0.3 m	5 Hz

Table 3. SLR measurement parameters (3sigma)

Then, the four system configurations are assessed:
- Standard optical (Ra/Dec measurements only)
- Standard optical + Nominal SLR
- Standard optical + High-accuracy SLR (H/A)
- Standard optical + High-frequency SLR (H/F)

Typical 3-minute path duration is considered for tracking and measurement of targets in LEO.

7.1 Simulation results and perspectives

Tab. 4 reports the final accuracy (3σ) obtained for each system configuration after 3-minute tracking of a typical sun-synchronous satellite at ~1000 km altitude.

	R *m*	I *m*	C *m*	Vr *cm/s*	Vi *cm/s*	Vc *cm/s*
Std opt.	384	232	316	43	307	22
Nom. SLR	5.9	5.5	6.7	5.9	3.8	6.6
H/A SLR	5.6	4.2	6.4	5.5	0.5	6.2
H/F SLR	4.4	4.1	5.5	3.9	0.3	5.0

Table 4. Final accuracy (3σ) vs. system configuration

Addition of the range measurement enables significant improvement in determination of both position and velocity. Major effect is shown on the in-track velocity due to the direct measurement of the radial position. The increase of the SLR measurement frequency slightly improves the final accuracy.

Influence of the SLR measurement parameters on the convergence speed is reported in Tab. 5, relatively to the accuracy obtained by the standard optical configuration after 3-minute tracking.

	R s	I s	C s	Vr s	Vi s	Vc s
Nom. SLR	4	2	2	49	16	82
H/A SLR	2	2	2	44	12	80
H/F SLR	1	1	1	43	7	77

Table 5. Duration required to reach the Std. optical accuracy vs. SLR configuration

Again, addition of the range measurement enables faster convergence of the OD algorithm – decreasing from minutes to seconds – compared to the standard optical configuration with angular measurement only. Further improvement of the convergence speed remains limited despite the 10-time ratio between the SLR measurement rates.

Therefore, the performance driver is clearly the combination of range measurement with standard angular measurements. That combination brings significant improvement of both the OD accuracy and convergence time with subsequent benefit for an operational SST system. Indeed, introduction of SLR systems in a SST network would enhance responsiveness and effectiveness in achieving on-demand tracking operations as: automated tracking can be initialized from standard TLE orbit with limited accuracy; combined measurements enable accurate refinement of the orbit data; time needed to reach relevant accuracy is reduced so that availability and opportunity for on-demand measurement is increased.

8 EXPERIMENTAL VALIDATION

In order to validate studies and models, Astrium has designed and operated an experimental SLR installation for non-cooperative target, in partnership with the GéoAzur laboratory of OCA [7].

OCA has been performing laser ranging measurements, from the South of the France, since 1969, and is a performing contributor to the International Laser Ranging Service (ILRS).

8.1 Experimental setup

The experimental setup is supported by the MéO station (Metrology and Optics) of OCA, one of the four lunar ranging stations in the world. The station features a 1.5m aperture Ritchey Chretien telescope used for both laser emission and detection, the optical commutation being performed by a rotating mirror. The direct-drive alt-az fork mount delivers pointing accuracy of 5 arcsec and maximal velocity of 5°/s.

To cope with non-cooperative targets, the MéO station has been installed a high energy laser source coupled with dedicated photo detection. Automated tracking and imaging are supported by a wide field-of-view (FoV) telescope in piggy-back position and an automatic tracking software.

A commercial-off-the-shelf (COTS) laser source, delivering 2 J per pulse at 532 nm, with a temporal width of 8 ns and a repetition rate of 10 Hz has been selected for the high energy laser source. Energy and impulse time are suitable to secure de link budget in nominal operation conditions, while wavelength and frequency are compatible with the reused equipments of the MéO station. A new SPAD detector, with larger sensitive surface, lower electronic noise, higher quantum efficiency and nanosecond temporal resolution has been implemented to allow extension of the temporal gate up to 60μs to cope with the 10km uncertainty of the TLE data.

The object initial detection and astrometry imaging is performed thanks to a small dioptric telescope coupled with a CCD camera as shown by Fig. 8.
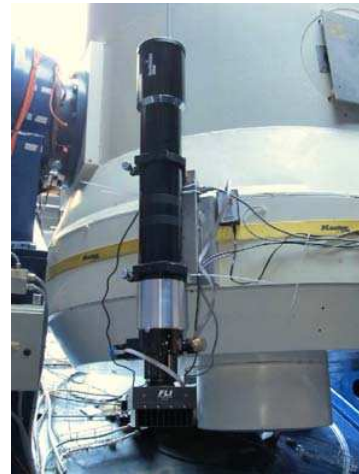
Figure 8. Piggy-back telescope and CCD camera mounted on the MéO telescope

The optical configuration delivers a 2.3° x 2.3° FoV for an Instantaneous FoV (IFOV) of 5.4 arcsec. The CCD camera allows a measurement rate of about 0,35 Hz with exposure time <100 ms and binning factor 2.

8.2 SLR campaigns

Preliminary SLR campaigns on cooperative targets using the regular MéO station were performed in 2010 to refine the link model and complete the trade-off.

Adaptation of the MéO station, integration tests and calibration were achieved during 2011 with first attempts on non-cooperative targets in December.

In March 2012, successful laser ranging on non-cooperative target was achieved and repeated over 10 targets in LEO as reported in Tab. 6.

ID	#NORAD	Period	Inc.	Apogee	Perigee	RCS
SL 14	20197	116.06	73.56	1522	1485	5.08
SL 14	20238	114.72	82.59	1474	1411	6.20
SL 14	16594	115.99	73.61	1522	1479	5.30
SL 19	37155	112.63	82.46	1502	1193	5.90
SL 8	14085	104.64	82.94	1003	952	6.30
Ariane 40	22830	100.65	98.71	798	781	9.70
SL 14	19196	116.00	73.59	1517	1485	5.60
SL 14	14522	115.98	73.61	1521	1479	5.20
SL 8	7443	117.76	74.03	1685	1475	5.80
SL 14	16144	114.75	82.60	1472	1416	7.10

Table 6. Target information

8.3 Verification of the link budget

Raw measurement in the time of flight of each echoed laser pulse associated with a timestamp in the target fly-by interval. Noise and subsequent false measurements need to be filtered before the number of detected photo-electrons per second can be counted.

Back to the link model defined by Eq. 1, all the parameters have been measured according to the experimental setup except the atmospheric attenuation computed by the Rozenberg equation and the OCS values deduced from the BRDF model. Range values are deduced from TLE data.

Comparison between theoretical computation and experimental results is given by Fig. 9, for several values of the OCS and the atmospheric attenuation (min, max and typical).
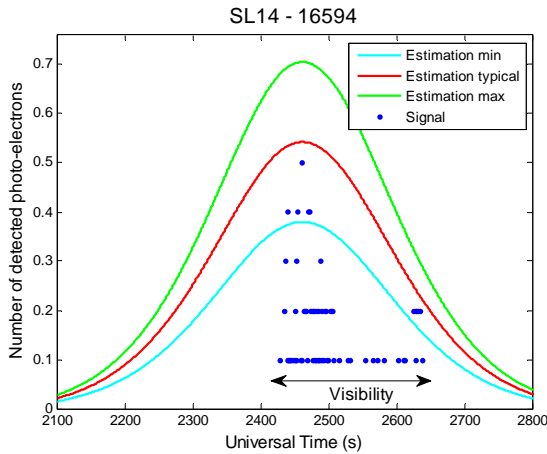
Figure 9. Theoretical vs. experimental link budget for SL14 16594

The OCS of the targets is considered as a parameter to make the experimental data fit with the theoretical curves. The deduced OCS values can afterward be cross-checked with photometric measurements,

numerical model from target size and shape or RCS values from external sources (e.g. NORAD).
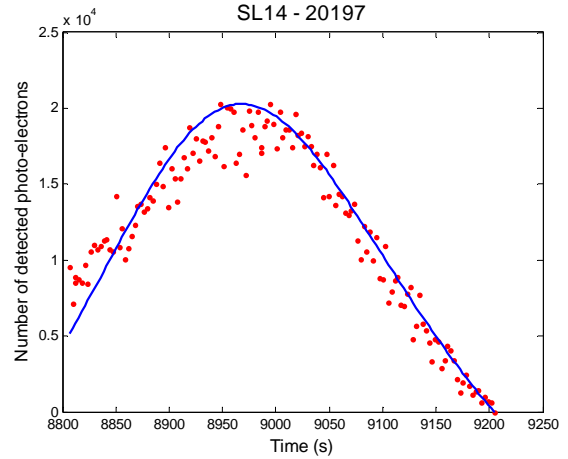
Figure 10. Light curve model (Lambertian sphere) vs. experiment considering for SL14 20197

Fig. 10 provides comparison between experimental OCS obtained by analysis of the astrometry images and estimation of the theoretical irradiation at the telescope aperture, considering a Lambertian scattering sphere.

The light curve model is verified to fit correctly the experimental light curves for 6 objects, using the BRDF of the target as the adjustment parameter.

Summary of assessment of the link budget is given through correspondence of the OCS values obtained by the different methods as reported in Tab. 7.

ID	#NORAD	OCS Theoretical	OCS Laser	OCS Light curve	RCS NORAD
SL 14	20197	25-40	20	7	5,08
SL 14	20238	25-40	40	7	6,2
SL 14	16594	25-40	140	29	5,3
SL 19	37155	ND	80	31	5,9
SL 8	14085	40-60	14	3	6,3
Ariane 40	22830	80-100	6	2	9,7
SL 14	19196	25-40	45	84	5,6
SL 14	14522	25-40	100	16	5,2
SL 8	7443	40-60	60	2	5,8
SL 14	16144	25-40	90	NA	7,1

Table 7. Correspondence of the OCS values

The theoretical OCS values are of the same order of magnitude than OCS obtained by laser ranging measurement. The wavelength dependence, as a function of the target material, may explained the large

difference between the NORAD RCS values and the optical OCS deduced from laser measurement. The wavelength dependence of the reflectance function may also explain the difference but roughly constant ratio between the OCS values obtained by active and passive measurements.

9 CONCLUSION

Astrium, in partnership with OCA, succeeded on March 2012 in achieving laser ranging on non-cooperative objects. Experimental measurements allowed consolidation of the studies and models developed by Astrium in the prospect to design an automated SLR station able to deliver value to an operational SST system. Key technologies and operation procedures have been implemented in real condition until demonstration of enhanced orbit determination of space debris in LEO [8].

Combination of laser ranging with conventional astrometry systems widens the scope of application for SST. Automated, responsive and accurate SLR systems could effectively support surveillance in LEO.

Challenges about SLR technology are both improvement of the link budget – to reduce misdetection and address small debris – and safe operation of high power laser for environment, air traffic and active satellite population.

10 REFERENCES

1. General Bernard MOLARD – "The Day After, A Quick switch from dream to nightmare is possible" – 16th ISU Annual International Symposium (2012)

2. John J DEGNAN – "Millimeter Accuracy Satellite Laser Ranging – A review" – Geodynamics Serine N°25 – 1993

3. Klein & Degnan – "Optical antenna gain 1: Transmitting antennas", Applied Optics 13, 2134, 1974

4. Min Seok OH & al. – "Systematic experiments for proof of Poisson statistics on direct-detection laser radar using Geiger mode avalanche photodiode" – Current Applied Optics 10,1041-1045 (2010)

5. M.G. Miller et al., "Turbulence environment characterization", RADC-79-131, Rome Air Devlopment Center (1979)

6. Victor P. Osweiler, Thesis report – "Covariance estimation and autocorrelation of Norad Two-Line Elements Sets" – Air Force Institute of Technology AFIT/GSS/ENY/06-M09 (2006)

7. Etienne Samain, Jocelyn Paris, Dominique Albanese, Hervé Haag, Thomas Lorblanches, Guillaume Blanchet, Jean-Marie Torre, Hervé Mariey, Bruno Esmiller, Sophie Vial, Myrtille Laas-Bourez, Xiaoni Wang, Pierre Exertier – "Demonstration and Interest of Laser Ranging on space debris, from the Grasse SLR station Article" – COSPAR (2012)

8. L. Hennegrave, M. Pyanet, H. Haag, G. Blanchet, B. Esmiller, S. Vial, E. Samain, J. Paris, D. Albanese – "Laser ranging with the MéO telescope to improve orbital accuracy of space debris" – SPIE Defense, Security & Sensing Conference (2012)